Spectroscopic properties of Er^{3+}/Yb^{3+} co-doped $50SiO_2–20Al_2O_3–30CaF_2$ glass and glass ceramics

2006 J. Phys.: Condens. Matter 18 6937

(http://iopscience.iop.org/0953-8984/18/29/030)

INSTITUTE OF PHYSICS PUBLISHING JOURNAL OF PHYSICS: CONDENSED MATTER

J. Phys.: Condens. Matter **18** (2006) 6937–6951 doi:10.1088/0953-8984/18/29/030

Spectroscopic properties of Er^{3+}/Yb^{3+} co-doped $50SiO_2$–$20Al_2O_3$–$30CaF_2$ glass and glass ceramics

Xvsheng Qiao[1], Xianping Fan[1,3], Minquan Wang[1], Jean-Luc Adam[2] and Xianghua Zhang[2]

[1] Department of Materials Science and Engineering, Zhejiang University, Hangzhou 310027, People's Republic of China
[2] UMR-CNRS 6512 'Verres & Ceramiques', Institut de Chimie de Rennes, Universite de Rennes 1-Campus de Beaulieu, 35042 Rennes Cedex, France

E-mail: fanxp@cmsce.zju.edu.cn

Received 15 February 2006
Published 6 July 2006
Online at stacks.iop.org/JPhysCM/18/6937

Abstract

A spectroscopic investigation of Er^{3+}/Yb^{3+} co-doped $50SiO_2$–$20Al_2O_3$–$30CaF_2$ glasses and transparent glass ceramics containing CaF_2 nanocrystals is presented. The formation of CaF_2 nanocrystals in the glass ceramic was confirmed by x-ray diffraction (XRD) and transmission electron microscopy (TEM). The Judd–Ofelt parameters of the Er^{3+} ions in the glass and glass ceramic have been calculated; they suggested that Er^{3+} ions had been incorporated into CaF_2 nanocrystals in the glass ceramics. The upconversion luminescence intensity of the Er^{3+}/Yb^{3+} co-doped glass ceramic was much stronger than that of the Er^{3+}/Yb^{3+} co-doped glass. The upconversion luminescence mechanism has been ascribed to a two-photon absorption process for the green and red luminescence and a three-photon absorption process for the blue luminescence.

1. Introduction

Er^{3+}-doped glasses have attracted great attention because of their potential applications in optoelectronic fields, such as glass lasers, optoelectronic communication devices, sensors and color displays [1–6]. Co-doping with Yb^{3+} can greatly enhance the luminescence intensity of Er^{3+} ions owing to the efficient energy transfer from the Yb^{3+}:$^2F_{5/2}$ to the Er^{3+}:$^4I_{11/2}$ state, because both Yb^{3+} and Er^{3+} ions have an absorption band around 980 nm and the absorption cross section of Yb^{3+} ions is much larger than that of Er^{3+} ions [7–9]. So far, researchers' efforts have already realized the commercialization of Er^{3+}/Yb^{3+} co-doped glass fibres and optical amplifiers. However, almost all these applied glasses are fluoride glasses, which have

[3] Author to whom any correspondence should be addressed.

some disadvantages in chemical and mechanical stabilities. Oxyfluoride glass ceramics doped with rare earth ions have been investigated widely in the past, since they possess not only higher chemical and mechanical stability than fluoride glass but also lower phonon energy than oxide glass [10]. Those glass ceramics usually contain such small crystalline phases as the nanosize $Pb_xCd_{1-x}F_2$ or PbF_2 crystals in the glass hosts that they can improve the optical properties with no loss of the transparency [11]. However, both CdF_2 and PbF_2 are toxic raw materials. CaF_2 is selected instead of CdF_2 and PbF_2 as one of the raw materials in the present study. CaF_2 is an important optical raw material with high solubility of both sensitizer and activator rare earth ions [12]. Recently, more interest has been focused on rare earth ion doped CaF_2 due to potential applications in optoelectronic devices. Extensive studies have been carried out on the optical properties of rare earth ion doped CaF_2 single crystals [13–17]. The same material as thin films deposited on Si substrates has also been studied [18, 19]. CaF_2:Er^{3+} optical waveguides grown by molecular beam epitaxy have recently been demonstrated [20–22]. Furthermore, crystalline CaF_2 is highly transparent from 0.13 to 9.5 μm and gives a better matching of refractive index with the aluminosilicate glassy host. This leads to possibilities of preparing transparent glass ceramics containing CaF_2 nanocrystals. This paper presents a detailed spectroscopic investigation of Er^{3+}/Yb^{3+} co-doped $50SiO_2$–$20Al_2O_3$–$30CaF_2$ glass and transparent glass ceramics containing CaF_2 nanocrystals. The formation of CaF_2 nanocrystals in the $50SiO_2$–$20Al_2O_3$–$30CaF_2$ glass is confirmed by XRD and TEM. The difference in oscillator strengths between glass and glass ceramics is discussed on the basis of a Judd–Ofelt intensity analysis. The upconversion luminescence and near-infrared luminescence of Er^{3+}/Yb^{3+} co-doped glasses and glass ceramics are described.

2. Experimental details

The 5 mol% YbF_3 and 0.5 mol% ErF_3 co-doped $50SiO_2$–$20Al_2O_3$–$30CaF_2$ oxyfluoride glasses were prepared from high purity SiO_2, Al_2O_3, CaF_2, YbF_3 and ErF_3 raw materials. The batches of the raw materials were melted at 1400 °C for 45 min in a covered corundum crucible in normal atmosphere. The melt was poured on a brass mould and then pressed by another brass plate. The glass samples (named as GErYb) were finally obtained. The glass ceramic samples (named as GCErYb) were prepared by heat treatment of the glasses for 2 h at 660 °C, chosen based on DTA measurements. In addition, the 0.5 mol% ErF_3 doped $50SiO_2$–$20Al_2O_3$–$30CaF_2$ oxyfluoride glasses (named as GEr) were also prepared in the same molten conditions. Then the glass and glass ceramic samples were polished on a UNIPOL-802 precision lapping/polishing machine. Glass and glass ceramic samples transparent in visible light were finally obtained.

DTA measurements were carried out in a CDR-1 differential thermal analyser in normal atmosphere in order to confirm the glass transition temperature (T_g) and crystallization peak temperature (T_x). X-ray diffraction measurements were performed with a XD-98 diffractometer with Cu Kα radiation at 4° min^{-1} scanning rate. TEM images were taken with a JEM4000 FX microscope (JEOL) and the TEM samples were prepared by mechanical polishing and subsequent ion-milling. Densities were measured using the Archimedes principle, with distilled water as the medium. Refractive indices were measured on a Metricom-2010 prism coupler at 632.8, 1300 and 1549 nm. Optical absorption measurements were performed on a Hitachi UV-4100 spectrophotometer. For luminescence spectra measurements: (1) direct luminescence spectra were measured with a slit resolution of 2.5 nm on a Hitachi F-4500 fluorescence spectrophotometer by excitation of a Xe lamp; (2) upconversion luminescence spectra were measured with a slit resolution of 1.0 nm on a Hitachi F-4500 fluorescence spectrophotometer using 980 nm excitation from a laser diode; (3) 980 nm (laser) excited near-

infrared luminescence and 1064 nm (laser) excited decay spectra were measured with a Horiba Triax-550 monochromator. All measurements were performed at room temperature.

3. Theoretical details

From the absorption spectrum, the oscillator strengths of the electronic transitions can be calculated using the expression

$$P_{\text{exp}} = \frac{2303mc^2}{\pi e^2 N_0} \int \varepsilon(\nu)\, \mathrm{d}\nu \tag{1}$$

where m is the electron mass (g) and e is the electron charge (electrostatic units), c is the velocity of light, N_0 is the Avogadro constant, and $\varepsilon(\nu)$ is the molar extinction coefficient at the wavenumber ν (cm^{-1}), which can be computed from the Beer–Lambert law:

$$\varepsilon(\nu) = \frac{\log(I_0/I)}{Cd} \tag{2}$$

where $\log(I_0/I)$ is the measured absorbance at the wavenumber ν (cm^{-1}), C is the concentration of the lanthanide ions ($\text{mol}/1000\ \text{cm}^3$) and d is the light path in the measured sample (cm) [23, 24].

According to the Judd–Ofelt theory [25, 26], the oscillator strength of the $aJ \rightarrow bJ'$ transition (at the wavenumber ν) can be calculated from

$$P_{\text{cal}} = P_{\text{ed}} + P_{\text{md}} = \frac{8\pi^2 mc\nu}{3h(2J+1)e^2n^2}\left(\chi_{\text{ed}} S_{\text{ed}} + \chi_{\text{md}} S_{\text{md}}\right) \tag{3}$$

where χ is the term for the effective field at a well-localized centre [27] in a medium of isotropic refractive index n, which for electric-dipole transitions and magnetic-dipole transitions, respectively, is given by

$$\chi_{\text{ed}} = \frac{n(n^2+2)^2}{9} \qquad \text{(for electric-dipole transitions)} \tag{4}$$

$$\chi_{\text{md}} = n^3 \qquad \text{(for magnetic-dipole transitions).} \tag{5}$$

The electric dipole and magnetic dipole, S_{ed} and S_{md}, are expressed as

$$S_{\text{ed}}(aJ, bJ') = e^2 \sum_{t=2,4,6} \Omega_t \left|\left\langle aJ \left| U^{(t)} \right| bJ' \right\rangle\right|^2 \tag{6}$$

$$S_{\text{md}}(aJ, bJ') = \frac{e^2}{4m^2c^2} \left|\left\langle aJ \left| L + 2S \right| bJ' \right\rangle\right|^2. \tag{7}$$

However, it must be noted that only the magnetic dipolar transitions, with selection rules $\Delta S = \Delta L = 0$, $\Delta J = 0, \pm 1$, could contribute efficiently to the oscillator strength of rare earth ions [28].

The Ω_t parameters, known as Judd–Ofelt (JO) parameters, can be determined from a least-squares fit to the values of measured oscillator strengths using equation (3). The reduced matrix elements of $|\langle aJ|U^{(t)}|bJ'\rangle|^2$ and the expression of $|\langle aJ|L+2S|bJ'\rangle|^2$ have been given by some researchers [1, 6]. A measure of the accuracy of the fit is given by the root-mean-square (rms) deviation:

$$\text{rms} = \left[\frac{\Sigma(P_{\text{cal}} - P_{\text{exp}})^2}{(\xi - 3)}\right]^{1/2} \tag{8}$$

where ξ is the number of transitions analysed.

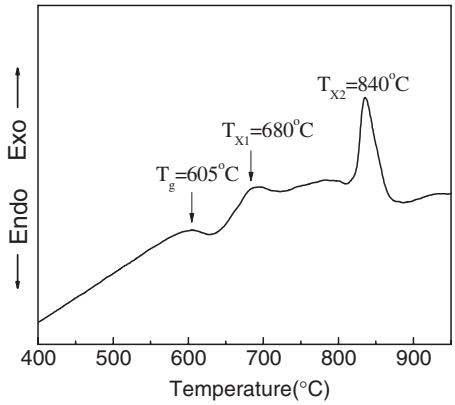

Figure 1. DTA curve of the 5 mol% YbF_3 and 0.5 mol% ErF_3 co-doped $50SiO_2$–$20Al_2O_3$–$30CaF_2$ glass.

The spontaneous emission probabilities $A(aJ, bJ')$ of the different electronic transitions are given in the Judd–Ofelt theory by

$$A(aJ, bJ') = A_{\mathrm{ed}} + A_{\mathrm{md}} = \frac{64\pi^4\nu^3}{3h(2J+1)}\left(\chi_{\mathrm{ed}}S_{\mathrm{ed}} + \chi_{\mathrm{md}}S_{\mathrm{md}}\right). \tag{9}$$

The emission branching ratio of a transition is defined as

$$\beta(aJ, bJ') = \frac{A(aJ, bJ')}{\sum_{bJ'} A(aJ, bJ')} \tag{10}$$

and the radiative lifetime of an emitting state is related to the total spontaneous emission probabilities for all transitions from this state by

$$\tau = \frac{1}{\sum_{bJ'} A(aJ, bJ')} \tag{11}$$

where the sum is extended over all the states at energies lower than aJ.

For direct excitation, the luminescence quantum yield, η, is defined as

$$\eta = \frac{\text{emitted light intensity}}{\text{absorbed radiation intensity}} = \frac{\tau_{\mathrm{exp}}}{\tau_{\mathrm{cal}}} \tag{12}$$

where τ_{exp} is the observed lifetime and τ_{cal} is the lifetime calculated from equation (11).

4. Results and discussion

Figure 1 shows the DTA curve of GErYb where T_{g} (590 °C), T_{X1} (680 °C) and T_{X2} (840 °C) stand for the glass transition temperature, and the first and the second crystallization temperature, respectively. XRD analysis showed that the first crystallization peak, T_{X1}, could be ascribed to the precipitation of CaF_2 crystals and the second crystallization peak, T_{X2}, to the bulk crystallization process of the glass matrix. Thus 660 °C, a little lower than T_{X1}, was selected as the heat treatment temperature for the precipitation of CaF_2 nanocrystals from the glassy matrix.

Figure 2 shows the XRD patterns of GErYb and GCErYb, respectively. GErYb is completely amorphous with no diffraction peaks. But the intense diffraction peaks were observed for the XRD curve of GCErYb, and these diffraction peaks can be easily assigned

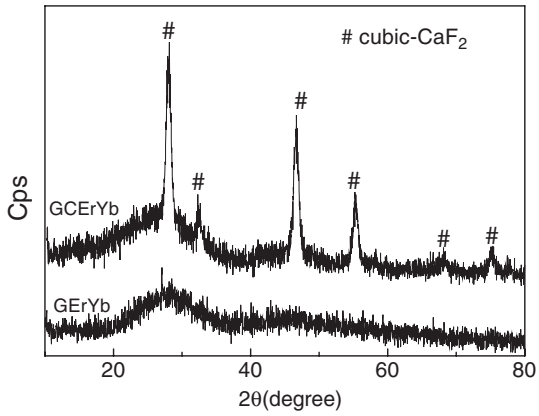

Figure 2. XRD pattern of Er^{3+}/Yb^{3+} co-doped glass (GErYb) and glass ceramic (GCErYb).

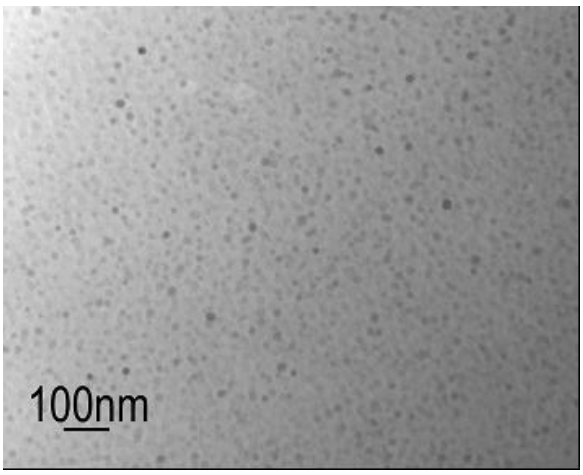

Figure 3. TEM image of Er^{3+}/Yb^{3+} co-doped glass ceramic.

to the CaF_2 cubic phase. From the obtained peak width of XRD pattern, the size of CaF_2 nanocrystals in GCErYb can be calculated by the Sherrer formula:

$$D_{hkl} = \frac{K\alpha}{\beta \cos\theta} \tag{13}$$

where D_{hkl} is the crystal size normal to (hkl), λ is the x-ray wavelength, θ is the angle of diffraction, β is the full-width at half-maximum (FWHM) of the diffraction peak and the constant $K = 0.90$. The CaF_2 crystal size can be calculated to be about 10 nm. Figure 3 shows a TEM image of the glass ceramic GCErYb. The size of the roughly spherical particles can be found to be approximately 10 nm, which is consistent with the Scherrer-calculated diameter.

Some physical properties of GErYb and GCErYb are presented in table 1. The refractive indices at 632.8, 1300 and 1549 nm were used to determine the relations between the refractive index and the wavelength by a least-squares fitting to the Sellmeier dispersion equation [29]

$$n^2(\lambda) = 1 + \frac{S\lambda^2}{\lambda^2 - \lambda_0^2}. \tag{14}$$

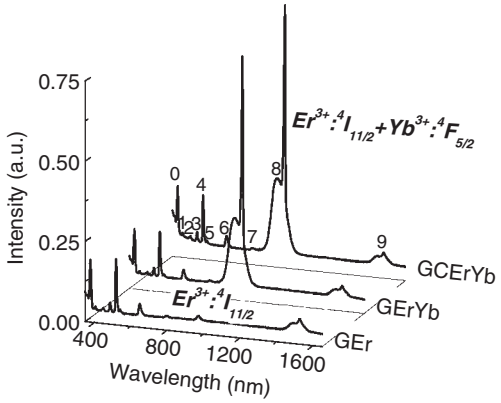

Figure 4. Absorption spectra of GEr, GErYb and GCErYb. The absorption bands were assigned to the transitions from the ground state to the state: (0) $^4G_{11/2}$; (1) $^2H_{9/2}$; (2) $^4F_{5/2,3/2}$; (3) $^4F_{7/2}$; (4) $^2H_{11/2}$; (5) $^4S_{3/2}$; (6) $^4F_{9/2}$; (7) $^4I_{9/2}$; (8) $^4I_{11/2}$; (9) $^4I_{13/2}$.

Table 1. Some physical properties of GErYb and GCErYb.

Sample name	GErYb	GCErYb
Density (g cm^{-3})	3.039	2.923
Thickness (cm)	0.060	0.061
Er^{3+} concentration (mol dm^{-3})	0.171	0.170
Refractive index (at 632.8 nm)	1.507	1.507
Refractive index (at 1300 nm)	1.510	1.510
Refractive index (at 1549 nm)	1.516	1.515

Table 2. The calculated refractive indices, n, and experimental and calculated oscillator strengths, P, of the Er^{3+} absorption transitions from the ground state $^4I_{15/2}$ to the [SL]J states (for GErYb: rms $= 1.52 \times 10^{-7}$; for GCErYb: rms $= 1.10 \times 10^{-7}$).

Excited	GErYb				GCErYb			
state	λ (nm)	n	$P_{exp} \times 10^8$	$P_{cal} \times 10^8$	λ (nm)	n	$P_{exp} \times 10^8$	$P_{cal} \times 10^8$
$^4I_{13/2}$	1531	1.533	168.6	166.7	1529	1.523	164.4	113.6
$^4I_{11/2}$	—	—	—	—	—	—	—	—
$^4I_{9/2}$	796	1.541	23.3	30.5	800	1.530	22.6	26.7
$^4F_{9/2}$	651	1.546	209.0	203.4	652	1.535	189.9	186.2
$^4S_{3/2}$	541	1.554	67.3	45.0	539	1.542	51.8	44.6
$^2H_{11/2}$	521	1.556	823.8	814.2	521	1.544	559.4	557.2
$^4F_{7/2}$	488	1.560	167.5	186.7	487	1.547	164.6	179.4
$^4F_{5/2,3/2}$	451	1.566	71.2	85.2	449	1.552	75.0	84.3
$^2H_{9/2}$	407	1.575	62.0	67.8	407	1.560	49.6	65.8
$^4G_{11/2}$	377	1.583	1455.3	1466.1	378	1.567	995.8	998.4

Using Sellmeier's dispersion equation, the refractive index could be recalculated at the specific wavelength. Table 2 shows the calculated refractive indices of the samples at the experimentally observed energy level positions of Er^{3+}, which were obtained from the absorption spectra as shown in figure 4. Compared with GEr, GErYb and GCErYb have a much stronger absorption band at 980 nm, which results from the $^2F_{7/2} \rightarrow {}^2F_{5/2}$ transition of Yb^{3+}. Figure 5 shows

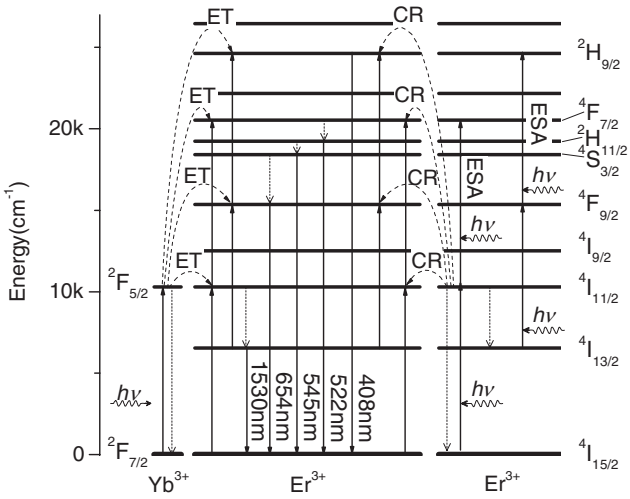

Figure 5. Energy diagram of Er^{3+} and Yb^{3+} ions and possible luminescence mechanisms under 980 nm excitation.

the possible sensitizing mechanism and the simplified energy level diagram of Er^{3+}/Yb^{3+}. When GErYb or GCErYb was excited at 980 nm, the energy transfer from Yb^{3+} to Er^{3+} via the reaction $^2F_{5/2}(Yb^{3+}) + {}^4I_{15/2}(Er^{3+}) \rightarrow {}^2F_{7/2}(Yb^{3+}) + {}^4I_{11/2}(Er^{3+})$ would act as indirect pumping of Er^{3+} and efficiently sensitize the luminescence of Er^{3+}.

In order to provide a quantitative interpretation of Er^{3+} spectral studies in the glass and glass ceramics, the oscillator strengths of all the absorption bands were experimentally measured using expression (1) and parametrically fitted with expression (3). And then the three JO parameters, Ω_t ($t = 2, 4, 6$), were obtained by a least-squares programming technique. Using the three JO parameters, the oscillator strengths of the Er^{3+} absorption bands could be recalculated in order to evaluate the accuracy of the fit by the root-mean-square (rms) deviation. Table 2 shows the experimental and calculated oscillator strengths, P, of the Er^{3+} absorption transitions in glass and glass ceramic. Smaller oscillator strengths in GCErYb can be observed in comparison with that in GErYb, which lead to smaller Ω_t parameters for GCErYb. The JO parameters Ω_t of the Er^{3+}/Yb^{3+} co-doped glass and glass ceramic, as well as other materials, are given in table 3. In general, Ω_2 decreases with the increase of symmetry between rare earth ions and the ligand fields and Ω_6 increases with the decrease of covalency between rare earth ions and the hosts [30–32]. In traditional glasses, the Ω_2 value decreases with the host changing from oxides to fluorides [33]. From table 3 it can found that the Ω_2 value of GCErYb was smaller than that of GErYb, which indicates that more Er^{3+} have entered into the CaF_2 nanocrystal phase in GCErYb. During the crystallization of CaF_2 nanocrystals, Er^{3+} ions acted as crystal nuclei. The Ca^{2+} ions were partially substituted by Er^{3+} ions. Thus, the Er^{3+} ions in the CaF_2 nanocrystal were mainly coordinated by F^- ions and a more ionic bond environment of the Er^{3+} ions can be expected in comparison with that in GErYb. Therefore, Er^{3+} ions have been incorporated into the CaF_2 nanocrystals in GCErYb, which ultimately resulted in the decrease of Ω_2. Together with Ω_6, Ω_4 has an effect on some transitions of Er^{3+}, such as the $^4S_{3/2} \rightarrow {}^4I_{15/2}$ transition. The spontaneous transitions of the $^4S_{3/2}$ state depend only on the Ω_4 and Ω_6 parameters due to the reduced matrix elements of the unit tensor $[U^{(2)}]^2$ that are equal to zero, as shown in table 4. Furthermore, for $^4S_{3/2} \rightarrow {}^4I_{15/2}$, $[U^{(4)}]^2$ is also zero. But $[U^{(4)}]^2$

Table 3. Values of Ω_t of the Er^{3+} ions in the investigated samples and other different glasses.

Hosts	$\Omega_2 \times 10^{20}$ (cm^2)	$\Omega_4 \times 10^{20}$ (cm^2)	$\Omega_6 \times 10^{20}$ (cm^2)	Ω_4/Ω_6
GErYb	5.19	1.59	1.16	1.37
GCErYb	3.37	1.40	1.15	1.22
ZBLAN[a]	2.91	1.27	1.11	1.14
ZBLA[b]	2.54	1.39	0.57	1.43
Fluorophosphate[c]	3.43	1.70	1.29	1.32
Fluorozirconate[b]	5.6	2.0	1.31	1.52
Phosphate[a]	6.65	1.52	1.11	1.37
CaF_2[b]	6.6	2.3	2.0	1.15
LaF_3[b]	3.9	1.0	2.3	0.43

[a] See reference [33].
[b] See reference [34].
[c] See reference [35].

Table 4. The reduced matrix elements of Er^{3+}.

Transition of Er^{3+}	$[U^{(2)}]^2$	$[U^{(4)}]^2$	$[U^{(4)}]^2$
$\mathbf{^4F_{9/2} \rightarrow {}^4I_{15/2}}$	**0.0000**	**0.5511**	**0.4621**
$^4F_{9/2} \rightarrow {}^4I_{13/2}$	0.0109	0.1533	0.0828
$^4F_{9/2} \rightarrow {}^4I_{11/2}$	0.0715	0.0101	1.2671
$^4F_{9/2} \rightarrow {}^4I_{9/2}$	0.1220	0.0061	0.0203
$\mathbf{^4S_{3/2} \rightarrow {}^4I_{15/2}}$	**0.0000**	**0.0000**	**0.2225**
$^4S_{3/2} \rightarrow {}^4I_{13/2}$	0.0000	0.0000	0.3419
$^4S_{3/2} \rightarrow {}^4I_{11/2}$	0.0000	0.0046	0.0773
$^4S_{3/2} \rightarrow {}^4I_{9/2}$	0.0000	0.0765	0.2569
$^4S_{3/2} \rightarrow {}^4F_{9/2}$	0.0000	0.0036	0.0014

still has a contribution on the other branching ratio for the $^4S_{3/2}$ luminescence. Therefore, small Ω_4 and large Ω_6 are necessary for the luminescence corresponding to $^4S_{3/2} \rightarrow {}^4I_{15/2}$ transition of Er^{3+}. In order to maximize the luminescence intensity of $^4S_{3/2} \rightarrow {}^4I_{15/2}$ compared with $^4S_{3/2} \rightarrow {}^4F_{9/2}$, $^4S_{3/2} \rightarrow {}^4I_{9/2}$, $^4S_{3/2} \rightarrow {}^4I_{11/2}$ and $^4S_{3/2} \rightarrow {}^4I_{13/2}$ transitions, one requires $\Omega_4 \ll \Omega_6$. Thus Ω_4/Ω_6 can be used to measure the visible laser corresponding to the $^4S_{3/2} \rightarrow {}^4I_{15/2}$ transition of Er^{3+}, which was first introduced by Kaminskii [36] for evaluating the infrared spectroscopic properties of Nd^{3+}. The smaller the value of Ω_4/Ω_6 is, the more intense the emission intensity of $^4S_{3/2} \rightarrow {}^4I_{15/2}$ transition is. From table 3 it can be found that the typical range of Ω_4/Ω_6 is 0.43–1.52. The smaller Ω_4/Ω_6 of GCErYb (1.22) in comparison with that of GErYb (1.37) indicated that GCErYb would exhibit the stronger green luminescence.

Table 5 shows the spontaneous emission probabilities, A, branching ratio, β_{ij}, and radiative lifetime, τ, of several Er^{3+} transitions from state [SL]J to state [S′L′]J′, which were calculated by using the expressions (9)–(11). Obviously, Er^{3+} in GCErYb has a longer radiative lifetime than in GErYb, and at the same time there were no changes of the branching ratios between GErYb and GCErYb. All the above factors, which suggest the probable inclusion of Er^{3+} into the CaF_2 nanocrystalline phase, ensure that GCErYb has the more favourable spectroscopic properties, which can be illustrated by the luminescence spectra as shown in figures 6–10.

Figure 6 shows the luminescence spectra (excited at 378 nm with a Xe lamp) of Er^{3+} in GEr, GErYb and GCErYb. Due to the lower phonon energy of the precipitated CaF_2 nanocystals in GCErYb, a new red emission at 655 nm ($^4F_{9/2} \rightarrow {}^4I_{15/2}$ transition) appeared,

Table 5. Spontaneous emission probabilities, A, branching ratio, β_{ij}, and radiative lifetimes, τ, of several Er^{3+} emission transitions from state [SL]J to state [S′L′]J′.

		GErYb				GCErYb			
[SL]J	[S′L′]J′	A_{ed} (s^{-1})	A_{md} (s^{-1})	β_{ij} (%)	τ (ms)	A_{ed} (s^{-1})	A_{md} (s^{-1})	β_{ij} (%)	τ (ms)
$^4I_{13/2}$	$^4I_{15/2}$	79	33	100	8.977	75	32	100	9.328
$^4I_{11/2}$	$^4I_{15/2}$	96		80	8.327	86		79	9.209
	$^4I_{13/2}$	15	9	20		14	9	21	
$^4I_{9/2}$	$^4I_{15/2}$	76		70	9.148	65		68	10.404
	$^4I_{13/2}$	31		28		29		30	
	$^4I_{11/2}$	1	2	2		1	2	2	
$^4F_{9/2}$	$^4I_{15/2}$	767		89	1.159	689		89	1.296
	$^4I_{13/2}$	46		5		39		5	
	$^4I_{11/2}$	47		5		42		5	
	$^4I_{9/2}$	3		0		2		0	
$^4S_{3/2}$	$^4I_{15/2}$	248		63	2.546	244		63	2.581
	$^4I_{13/2}$	114		29		113		29	
	$^4I_{11/2}$	10		3		10		3	
	$^4I_{9/2}$	20		5		20		5	
	$^4F_{9/2}$	0		0		0		0	
$^2H_{11/2}$	$^4I_{15/2}$	4855		94	0.195	3270		94	0.287
	$^4I_{13/2}$	96		2		76		2	
	$^4I_{11/2}$	62		1		48		1	
	$^4I_{9/2}$	99		2		74		2	
	$^4F_{9/2}$	26		1		17		1	
	$^4S_{3/2}$	0		0		0		0	
$^4F_{7/2}$	$^4I_{15/2}$	1276		73	0.569	1211		74	0.608
	$^4I_{13/2}$	250		14		217		13	
	$^4I_{11/2}$	129		7		117		7	
	$^4I_{9/2}$	86		5		82		5	
	$^4F_{9/2}$	4	13	1		3	14	1	
	$^4S_{3/2}$	0		0		0		0	
	$^2H_{11/2}$	1		0		0		0	
$^4G_{11/2}$	$^4I_{15/2}$	17 246		85	0.050	11 467		84	0.073
	$^4I_{13/2}$	1739		9		1364		10	
	$^4I_{11/2}$	80		0		70		1	
	$^4I_{9/2}$	242		1		163		1	
	$^4F_{9/2}$	750		4		483		4	
	$^4S_{3/2}$	63		0		53		0	
	$^2H_{11/2}$	23		0		20		0	
	$^4F_{7/2}$	42		0		29		0	
	$^4F_{5/2}$	5		0		4		0	
	$^4F_{3/2}$	7		0		6		0	
	$^2H_{9/2}$	3	33	0		2		0	

the green emission at 545 nm presented stark split peaks and the blue emission at 408 nm ($^2H_{9/2} \rightarrow {}^4I_{15/2}$ transition) became more intense in the emission spectra of GCErYb. The ratio of 545 nm ($^4S_{3/2} \rightarrow {}^4I_{15/2}$ transition) emission intensity to 522 nm ($^2H_{11/2} \rightarrow {}^4I_{15/2}$ transition) emission intensity significantly increases in GCErYb in comparison with that in GEr and GErYb. It is considered that $^2H_{11/2}$ as well as $^4S_{3/2}$ is populated from upper levels

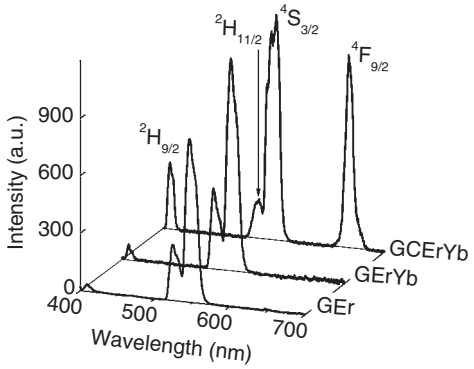

Figure 6. 378 nm (Xe lamp) excited luminescence spectra of Er^{3+} doped glass (GEr), Er^{3+}/Yb^{3+} co-doped glass (GErYb) and glass ceramic (GCErYb).

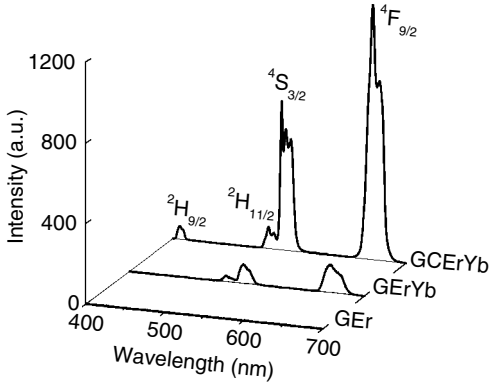

Figure 7. 980 nm (laser) excited upconversion luminescence spectra of Er^{3+} doped glass (GEr), Er^{3+}/Yb^{3+} co-doped glass (GErYb) and glass ceramic (GCErYb).

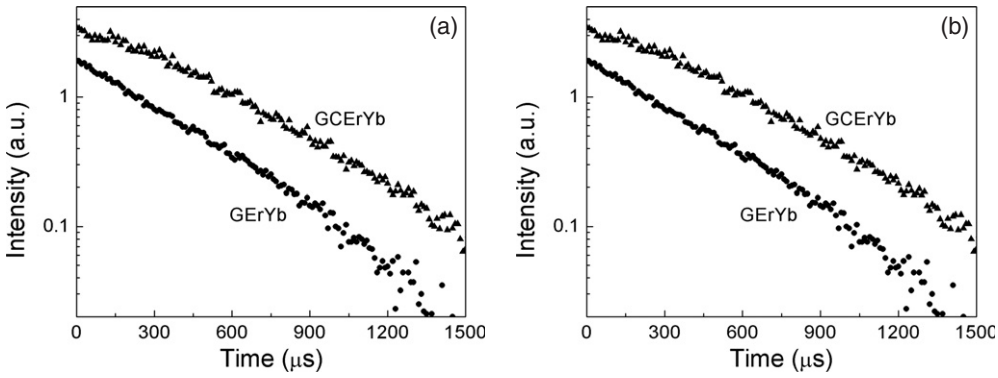

Figure 8. 1064 nm (laser) excited 545 nm luminescence (a) and 655 nm luminescence (b) decay curves of the Er^{3+}/Yb^{3+} co-doped glass (GErYb) and glass ceramic (GCErYb).

by multiphonon relaxation and that these two levels are coupled by a fast thermal equilibrium. The above processes then produces two emissions, centred at 522 and 545 nm, respectively. An analysis based on a simple three-level system comprised of $^4I_{15/2}$, $^4S_{3/2}$ and $^2H_{11/2}$ predicts

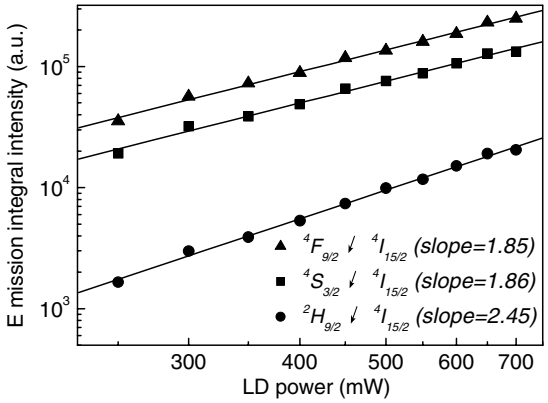

Figure 9. Dependence of the upconversion luminescence integral intensity of Er^{3+}/Yb^{3+} co-doped glass ceramic on the LD pumping power.

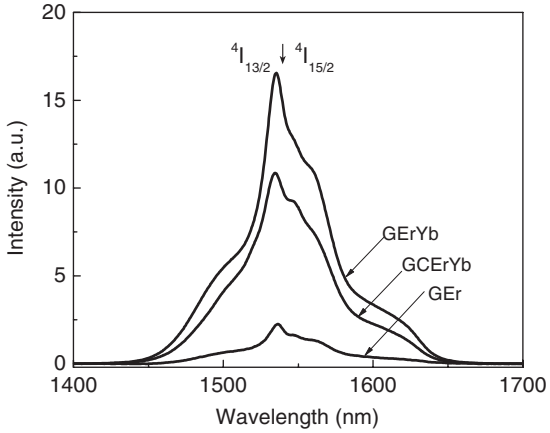

Figure 10. 980 nm (laser) excited near infrared luminescence spectra of Er^{3+} doped glass (GEr), Er^{3+}/Yb^{3+} co-doped glass (GErYb) and glass ceramic (GCErYb).

that thermalization of the $^2H_{11/2}$ level can be expressed by the following equation:

$$\frac{I_3}{I_4} = \frac{p_3 g_3 \hbar\omega_3}{p_4 g_4 \hbar\omega_4} \exp\left(\frac{E_{43}}{kT}\right), \tag{15}$$

where the p are the total spontaneous emission rates (the reciprocal of the lifetime, $1/\tau$), $\hbar\omega$ the photon energies, and g the degeneracies $(2J+1)$ of the corresponding energy level, respectively. The I terms represent the integrated intensity of a given transition at the temperature T. The E_{43} term is the energy gap between the $^4S_{3/2}$ and $^2H_{11/2}$ levels and k is Boltzmann's constant [37]. For GCErYb, g_3, g_4, $\hbar\omega_3$, $\hbar\omega_4$ and E_{43} are almost the same as those of GCErYb, so the value of I_3/I_4 is determined by the value of p_3/p_4 or τ_4/τ_3, and is positively correlated with p_3/p_4 or τ_4/τ_3. The calculated values of τ_4/τ_3 from table 5 are 0.077 for GErYb and 0.111 for GCErYb; therefore, lifetime variation led to the inversion of intensity ratio $(^4S_{3/2} \rightarrow {}^4I_{15/2})/(^2H_{11/2} \rightarrow {}^4I_{15/2})$.

Figure 7 shows the upconversion luminescence spectra (excited at 980 nm) of the Er^{3+}/Yb^{3+} co-doped glass (GErYb) and the glass ceramic (GCErYb), as well as the Er^{3+}-doped glass (GEr). It presents a similar character as figure 6. The emission bands can be

Table 6. The measured lifetime, τ_{exp}, and the luminescence efficiency, η, of the $^4S_{3/2}$ and $^4F_{9/2}$ levels for Er^{3+} in GErYb and GCErYb.

Sample name	$^4S_{3/2}$(545 nm)			$^4F_{9/2}$(655 nm)		
	τ_{exp} (ms)	τ_{cal} (ms)	η(%)	τ_{exp} (ms)	τ_{cal} (ms)	η (%)
GErYb	0.366	2.546	14.38	0.374	1.159	32.27
GCErYb	0.390	2.581	15.11	0.505	1.296	38.97

assigned to $^2H_{9/2} \rightarrow {}^4I_{15/2}$ (408 nm), $^2H_{11/2} \rightarrow {}^4I_{15/2}$ (522 nm), $^4S_{3/2} \rightarrow {}^4I_{15/2}$ (545 nm) and $^4F_{9/2} \rightarrow {}^4I_{15/2}$ (655 nm) transitions, respectively. For Er^{3+}-doped glass, no upconversion luminescence can be observed. However, intense upconversion luminescence can be observed for Er^{3+}/Yb^{3+} co-doped glass and glass ceramic. The green and red emissions were so bright that they could be visible to the naked eye when a laser beam of typically 50 mW was used for excitation. This indicates that an effective $Yb^{3+} \rightarrow Er^{3+}$ energy transfer upconversion takes place. Furthermore, the upconversion luminescence intensity of GCErYb was much stronger than that of GErYb and the blue upconversion luminescence (408 nm) of GCErYb could also be observed. This can be attributed to the lower phonon energy in the glass ceramic, where Er^{3+} and Yb^{3+} ions are incorporated into CaF_2 nanocrystals. The clear split emission peaks of GCErYb shown in figure 7 also suggest that some Er^{3+} ions are incorporated into CaF_2 nanocrystals. Thus much stronger upconversion luminescence of GCErYb can be obtained.

The above phenomenon can be further confirmed by measuring the luminescence decay curves of Er^{3+} that are given in figure 8. These curves are well fitted with first-order exponential decay and can be used to measure the lifetime of excited states. Then the luminescence efficiencies are obtained by using expression (12). Table 6 shows the measured lifetime, τ_{exp}, and the luminescence efficiency, η, of the $^4S_{3/2}$ and $^4F_{9/2}$ levels for Er^{3+} in GErYb and GCErYb. The lifetime, τ_{exp}, of the $^4S_{3/2}$ and $^4F_{9/2}$ levels in GCErYb were longer than that in GErYb, which can be attributed to a decreased non-radiative multi-phonon relaxation due to the lower phonon energy around Er^{3+} in GCErYb. Therefore, the luminescence efficiencies were improved in GCErYb.

In upconversion processes, the relation between the emission intensity I_{em} and the IR excitation intensity I_{ex} is the following:

$$I_{em} \propto (I_{ex})^n \tag{16}$$

where n is the number of IR photons absorbed per visible photon emitted. Therefore, a plot of $\log(I_{em})$ versus $\log(I_{ex})$ should yield a straight line with slope n. Figure 9 shows the dependence of the upconversion integral luminescence intensity of GCErYb on the LD pumping power. The slope of $^2H_{9/2} \rightarrow {}^4I_{15/2}$, $^4S_{3/2} \rightarrow {}^4I_{15/2}$ and $^4F_{9/2} \rightarrow {}^4I_{15/2}$ emission was 2.45, 1.86 and 1.85, respectively. This result indicated that the $^4S_{3/2} \rightarrow {}^4I_{15/2}$ and $^4F_{9/2} \rightarrow {}^4I_{15/2}$ transitions were related to a two-photon process and upconversion luminescence corresponding to the $^2H_{9/2} \rightarrow {}^4I_{15/2}$ transition could be ascribed to three-photon process.

For the green luminescence (at 522 and 545 nm), the possible upconversion luminescence mechanisms of the Er^{3+} ions can be described by: (1) excited state absorption (ESA), and (2) energy transfer upconversion (ETU) concluding cross relaxation (CR) between two Er^{3+} ions and energy transfer (ET) between Er^{3+} ions and Yb^{3+} ions. In these mechanisms, the 4f-electrons of Er^{3+} ions at the ground state are excited to the excited state $^4I_{11/2}$ by ground state absorption (GSA), CR from adjacent Er^{3+} ions and ET from Yb^{3+}. Then they can be excited to the $^4F_{7/2}$ level by similar ways of ESA, CR and ET. Finally, the electrons populated rapidly from the $^4F_{7/2}$ level to $^4S_{3/2}$, $^2H_{11/2}$ levels by multi-phonon relaxation, which produces two

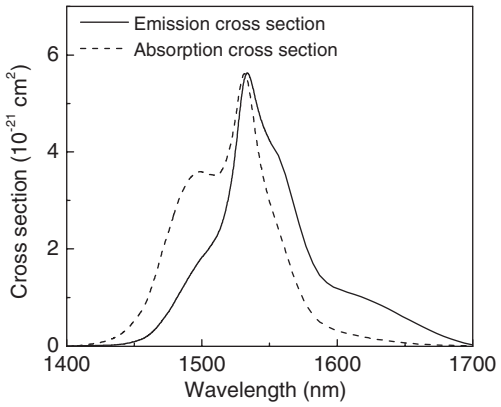

Figure 11. Absorption cross section and emission cross section of Er^{3+}/Yb^{3+} co-doped glass ceramic.

green luminescences, at 522 nm ($^2H_{11/2} \rightarrow {}^4I_{15/2}$) and 545 nm ($^4S_{3/2} \rightarrow {}^4I_{15/2}$). All the above processes have been illustrated in figure 5. ET from Yb^{3+} is dominating in the upconversion luminescence of Er^{3+}/Yb^{3+} co-doped glass and glass ceramic because Yb^{3+} has much larger absorption cross section than Er^{3+} around 980 nm. The upconversion luminescence of Er^{3+} ions is usually baffled by the multiphonon relaxation because there are many metastable energy levels between $^4S_{3/2}$, $^2H_{11/2}$ levels and the ground state. The multiphonon relaxation probability depends primarily upon the energy gap between two successive levels and the phonon energy of the host [38, 39]. The lower the phonon energy of host is, the smaller the multiphonon relaxation probability is. Due to much smaller phonon energy of CaF_2 nanocrystals ($\sim$280 cm^{-1}) [17] than silicate ($\sim$1100 cm^{-1}), the upconversion luminescence of Er^{3+} ions in the CaF_2 nanocrystals will be stronger than that in the glasses. Thus the upconversion luminescence intensity increased significantly from GErYb to GCErYb.

The electrons on the $^4I_{11/2}$ level can also relax to $^4I_{13/2}$ by non-radiative multi-phonon relaxation, which will lead to three emissions as shown in figure 5: (1) producing 1530 nm emission by the $^4I_{13/2} \rightarrow {}^4I_{15/2}$ transition; (2) producing 655 nm emission via the $^4I_{11/2} \rightarrow {}^4F_{9/2} \rightarrow {}^4I_{15/2}$ process by absorbing one photon (besides, the $^4S_{3/2} \rightarrow {}^4F_{9/2}$ non-radiative relaxation may also produce 655 nm emission); (3) producing 408 nm emission via the $^4I_{11/2} \rightarrow {}^4F_{9/2} \rightarrow {}^2H_{9/2} \rightarrow {}^4I_{15/2}$ process by absorbing other two photons. It is obvious that the $^4I_{11/2}$ level plays an important role in all the above upconversion processes. Figure 10 shows the near-infrared luminescence spectra (excited at 980 nm) of the Er^{3+} ions in GEr, GErYb and GCErYb. The emission band can be assigned to $^4I_{13/2} \rightarrow {}^4I_{15/2}$ transition. From the Er^{3+}-doped glass to the Er^{3+}/Yb^{3+} co-doped glass and glass ceramic, the near-infrared luminescence became significant increased due to the efficient energy transfer from Yb^{3+} to Er^{3+}, which ensures their application in 1530 nm optical communication. However, the 1530 nm emission of GCErYb was found to be weaker than that of GErYb. As in the above discussion, the $^4I_{11/2}$ level plays an important role in the 980 nm excited upconversion processes. When excited with a 980 nm laser, many more Er^{3+} 4f-electrons at $^4I_{11/2}$ in GCErYb were excited to the $^4F_{7/2}$ state than those in GErYb. Thus the Er^{3+} 4f-electrons at $^4I_{13/2}$ by relaxation from $^4I_{11/2}$ were much fewer in GCErYb, which resulted in weaker near-infrared emission of GCErYb in comparison with that of GErYb. For evaluating the stimulated emission properties of Er^{3+} in GCErYb, figure 11 shows the calculated stimulated emission cross sections and the absorption cross sections of GCErYb that were determined from the absorption spectrum. The emission

Table 7. Spectroscopic parameters of the $^4I_{13/2} \rightarrow {}^4I_{15/2}$ transition for Er^{3+} in GCErYb, fluorosilicate and ZBLAN hosts.

Hosts	σ_e ($\times 10^{-21}$ cm^{-1})	τ (ms)	FWHM (nm)	$\sigma \times \tau$	FWHM $\times \sigma_e$
GCErYb	5.6	9.3	71	52	398
Fluorosilicate[a]	7.5	11.0	53	82	398
ZBLAN[a]	5.1	9.5	65	49	331

[a] See reference [41].

cross sections were calculated from the absorption cross sections and the emission spectrum by McCumber theory [40]. The maximum emission cross section is 5.6×10^{-21} cm^{-1}, which has been listed in table 7. Er^{3+} in GCErYb has very similar emission cross sections and can provide broader bandwidth at about 1530 nm in comparison with ZBLAN and fluorosilicate. Thus the Er^{3+}/Yb^{3+} co-doped glass ceramic may be a candidate material for near-infrared optoelectronic communication devices.

5. Conclusions

Er^{3+}/Yb^{3+} co-doped transparent oxyfluoride glass ceramics containing CaF_2 nanocrystals have been prepared by the heat treatment of the 5 mol% YbF_3 and 0.5 mol% ErF_3 co-doped $50SiO_2$–$20Al_2O_3$–$30CaF_2$ glasses. Infrared-to-visible upconversion and 1530 nm infrared luminescence in the Er^{3+}/Yb^{3+} co-doped glass and glass ceramics have been observed under 980 nm excitation. The Judd–Ofelt parameters suggested that Er^{3+} ions had been incorporated into CaF_2 nanocrystals in the Er^{3+}/Yb^{3+} co-doped glass ceramics, which resulted in significant increase of the upconversion luminescence intensity of the Er^{3+}/Yb^{3+} co-doped glass ceramic in comparison with the Er^{3+}/Yb^{3+} co-doped glass. The red and green upconversion luminescence can be ascribed to a two-photon absorption process and the blue upconversion luminescence to a three-photon absorption process.

Acknowledgments

The authors gratefully acknowledge support for this research from the National Nature Science Foundation of China (No 50472062). This work has also benefitted from the Franco-Chinese cooperation programs PRA MX03-01 and PICS 92/0312.

References

[1] Oliveira A S, De Araujo M T, Gouveia-Neto A S, Sombra A S B, Medeiros Nneto J A and Aranha N 1998 *J. Appl. Phys.* **83** 604
[2] Collins S F, Baxter G W, Wade S A, Sun T, Grattan K T V, Zhang Z Y and Palmer A M 1998 *J. Appl. Phys.* **84** 4649
[3] Xie P and Gosnell T R 1995 *Opt. Lett.* **20** 1014
[4] Downing E, Hesselink L, Ralston J and Macfarlane R 1996 *Science* **73** 1185
[5] Man S O, Pun E Y B and Chung P S 2000 *Appl. Phys. Lett.* **77** 483
[6] Lande D, Orlov S S, Akella A, Hesselink L and Neurgaonkar R R 1997 *Opt. Lett.* **22** 1722
[7] Sardar D K, Gruber J B, Zandi B, Hutchinson J A and Trussell C W J 2003 *Appl. Phys.* **93** 2041
[8] Strohhöfer C and Polman A 2003 *Opt. Mater.* **21** 705
[9] Strohhöfer C and Polman A 2001 *J. Appl. Phys.* **90** 4314
[10] Qiao X S, Fan X P, Wang M Q and Zhang X H 2004 *Opt. Mater.* **27** 597
[11] Wang Y and Ohwaki J 1993 *Appl. Phys. Lett.* **63** 3268
[12] Caldiño U G 2003 *J. Phys.: Condens. Matter* **15** 7127

[13] Pollack S A 1964 *J. Chem. Phys.* **40** 2751
[14] Voronko Yu K, Zverev G M, Meshkov B B and Smirnov A I 1965 *Sov. Phys.—Solid State* **6** 2225
[15] Voronko Yu K, Kaminskii A A and Osiko V V 1966 *Sov. Phys.—JETP* **23** 10
[16] Zverev G M and Smirnov A I 1968 *Sov. Phys.—Solid State* **9** 1586
[17] Kumar G A, Riman R, Chae S C, Jang Y N, Bae I K and Moon H S 2004 *J. Appl. Phys.* **95** 3243
[18] Daran E, Bausa L E, Munoz-Yague A and Fontaine C 1993 *Appl. Phys. Lett.* **62** 2616
[19] Barriere A S, Raoux S, Garcia A, L'Haridon H, Lambert B and Moutonnet D 1994 *J. Appl. Phys.* **75** 1133
[20] Bausa L E, Lifante G, Daran E and Pernas P L 1996 *Appl. Phys. Lett.* **68** 3242
[21] Marco de Lucas M C, Daran E, Jacquier B, Garapon C, Mugnier J, Pernas P and Yague A M 1998 *J. Appl. Phys.* **83** 3345
[22] Daran E, Legros R, Munoz Yague A, Fontaine C and Bausa L E 1994 *J. Appl. Phys.* **76** 270
[23] Carnall W T, Crosswhite H and Crosswhite H M 1977 Energy level structure and transition probabilities of the trivalent lanthanides in LaF_3 *Argonne Natl. Lab. Rept.*
[24] Weber M J 1967 *Phys. Rev.* **157** 262
[25] Judd B R 1962 *Phys. Rev.* **127** 750
[26] Ofelt G S 1962 *J. Chem. Phys.* **37** 511
[27] Shinn M D, Sibley W A, Drexhage M G and Brown R N 1983 *Phys. Rev.* B **27** 6635
[28] Carnall W T, Fields P R and Wybourne B G 1965 *J. Chem. Phys.* **42** 3797
[29] Driscoll W G and Vauphan W 1978 *Handbook of Optics* (New York: McGraw-Hill)
[30] Tanabe S, Ohyagi T, Soga N and Hanada T 1992 *Phys. Rev.* B **46** 3305
[31] Tanabe S, Hayash H, Hanada T and Onodera N 2002 *Opt. Mater.* **19** 343
[32] Heidepriem H E, Ehrt D, Bettinelli M and Speghini A 1998 *J. Non-Cryst. Solids* **240** 66
[33] Zou X and Izumitani T 1993 *J. Non-Cryst. Solids* **162** 68
[34] Kumar G A, Riman R, Chae S C, Jang Y N, Bae I K and Moon H S 2004 *J. Appl. Phys.* **95** 3243
[35] Zemon S, Lambert G, Andrew L J, Miniscalco W J, Hall B T, Wei T and Folweiler R C 1991 *J. Appl. Phys.* **69** 6799
[36] Kaminskii A A 1996 *Crystalline Lasers: Physical Process and Operating Schemes* (New York: CRC Press)
[37] Xu S, Yang Z, Zhang J, Wang G, Dai S, Hu L and Jiang Z 2004 *Chem. Phys. Lett.* **385** 263
[38] Weber M J 1968 *Phys. Rev.* **171** 283
[39] Reisfeld R, Boehm L, Eckstein Y and Lieblich N 1975 *J. Lumin.* **10** 193
[40] Miniscalco W J and Quimby R S 1991 *Opt. Lett.* **16** 258
[41] Jha M, Shen S and Naftaly M 2000 *Phys. Rev.* B **62** 6215